analytical chemistry

pubs.acs.org/ac Article

Sensitive Dual-Mode Biosensors for CYFRA21-1 Assay Based on the Dual-Signaling Electrochemical Ratiometric Strategy and "On−Off−On" PEC Method

Qingqing Zhang, Yamin Fu, Ke Xiao, Cuicui Du, Xiaohua Zhang, and Jinhua Chen*

Cite This: *Anal. Chem.* 2021, 93, 6801−6807 Read Online

ACCESS | Metrics & More | Article Recommendations | Supporting Information

ABSTRACT: Herein, an electrochemical (EC)−photoelectrochemical (PEC) dual-mode biosensor was constructed for cytokeratin 19 fragment 21-1 (CYFRA21-1) assay based on the dual-signaling electrochemical ratiometric strategy and "on−off−on" PEC method. The indium tin oxide (ITO) electrode was modified by 3,4,9,10-perylenetetracarboxylic dianhydride (PTCDA)@C_{60} and gold nanoparticles (Au NPs), and the double-stranded DNA composed of thiol/methylene blue (MB)-labeled single-stranded DNA (ssDNA) (S0-MB) and antibody/ferrocene (Fc)-labeled ssDNA (Ab1-S1-Fc) was immobilized on the Au NPs/PTCDA@C_{60}/ITO electrode via the Au−S bond between Au NPs and thiol of S0-MB. With the help of another antibody-labeled ssDNA (Ab2-S2), the presence of CYFRA21-1 triggered a typical antigen−antibody sandwich immune reaction (Ab1, CYFRA21-1, and Ab2) and proximity hybridization between Ab1-S1-Fc and Ab2-S2. This caused the release of Ab1-S1-Fc from the modified electrode and the change of S0-MB to a hairpin structure, resulting in a decrease (an increase) of the oxidation peak current of Fc (MB) and an increase of the photocurrent due to the enhancing (inhibiting) effect of MB (Fc) on the photoelectric performance of the Au NPs/PTCDA@C_{60}/ITO electrode. Thus, CYFRA21-1 was detected by the developed EC−PEC dual-mode sensing platform sensitively, and the linear response ranges of 0.001−40 ng/mL with a detection limit of 0.3 pg/mL for the EC technique and 0.0001−4 ng/mL with a detection limit of 0.03 pg/mL for the PEC method were obtained. Furthermore, by changing the specific antibodies of disease-related biomarkers, the developed dual-mode biosensing platform could be readily extended to detect other antigens, implying its great potential applications in biological analysis and early disease diagnosis.

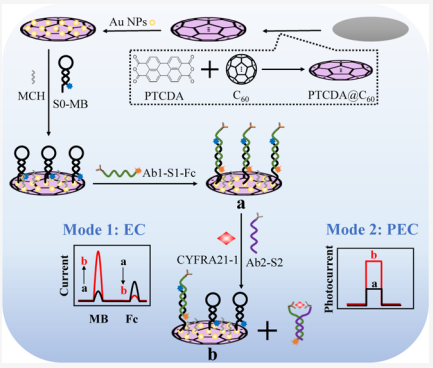

INTRODUCTION

Highly sensitive and reliable assay of disease-related biomarkers is a crucial challenge in early diagnosis, monitoring, and prognosis of a disease.[1] To date, many methods with a single response mechanism have been developed for the quantitative assays of disease-related biomarkers with high sensitivity, such as electrochemistry (EC),[2] photoelectrochemistry (PEC),[3] colorimetry (CL),[4] electrochemiluminescence (ECL),[6] and fluorescence (FL),[7] and using an electrochemical quartz crystal microbalance (EQCM).[5] However, the quantitative determination relying on single-mode readout may suffer from the effects of possibly co-existing interferents, different operators, apparatus, and nonstandard assay processes.[8]

To solve the above problems, dual-mode sensing platforms have recently been developed based on two different response mechanisms and relatively independent signal transduction, such as EC−PEC,[8] ECL−FL,[9] and PEC−CL.[10] The dual-mode sensing strategies not only possess the inherent characteristics of each response mode but also offer the mutual verification of the assay results obtained from different modes, which will effectively improve the accuracy and reliability of detection.[11−13] Among these developed dual-mode sensing platforms, EC−PEC dual-mode assay has received wide attention due to the following merits, such as fast response, high sensitivity, good selectivity, easy portability, and low cost.[14,15] Interestingly, the EC−PEC dual-mode platform needs only one electrochemical instrument, but has two signal readouts, providing the sensing platform with the advantages of a simple sensing structure.

Recently, a new electrochemical assay strategy, ratiometric electrochemical assay with both "signal-on" and "signal-off" signal readouts, has been reported.[16−18] The ratiometric electrochemical method can provide built-in correction and circumvent fluctuations in the signal caused by complex experimental conditions through its self-reference capability,[19,20] and thus exhibits enhanced reproducibility, stability,

Received: February 18, 2021
Accepted: April 12, 2021
Published: April 21, 2021

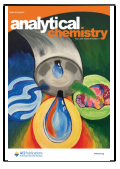

https://doi.org/10.1021/acs.analchem.1c00746
Anal. Chem. 2021, 93, 6801−6807

sensitivity, and anti-interference ability,[21,22] and has received wide attention.

On the other hand, PEC analysis has attracted great interest in recent years due to its excellent analytical performance originating from the complete separation between the excitation source (light energy) and detection signal (electric signal).[23−26] Various PEC biosensors have been developed and applied in many fields, such as DNA analysis,[27] enzymatic sensing,[28,29] heavy metal ion detection,[30] and immunoassays.[31] Recently, the on−off−on PEC strategy has received strong attention due to the integration of the signal quenching and amplification process, which ingeniously avoids the shortcomings of efficient PEC biological analysis.[32,33]

Considering the above findings, a new all-in-one dual-mode biosensing platform for the sensitive assay of protein biomarkers has been developed based on the dual-signaling electrochemical ratiometric strategy and on−off−on PEC method. Here, cytokeratin 19 fragment 21-1 (CYFRA21-1) was selected as a model due to its important role in the early diagnosis of non-small cell lung cancer (NSCLC).[34,35] As shown in Scheme 1, the indium tin oxide (ITO) electrode was

Scheme 1. Schematic Illustration of the Dual-Mode Sensing Platform for CYFRA21-1 Assay

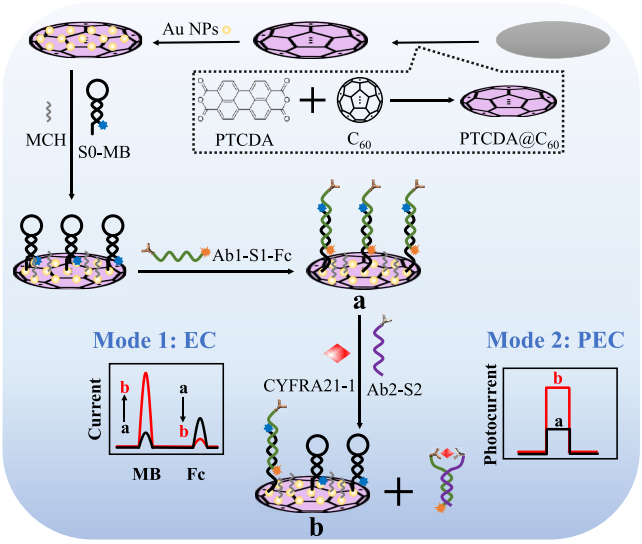

modified with 3,4,9,10-perylenetetracarboxylic dianhydride (PTCDA)@fullerene (C_{60}) and gold nanoparticles (Au NPs), and the hairpin structure single-stranded DNA (ssDNA) (S0-MB) was immobilized on the Au NPs/PTCDA@C_{60}/ITO electrode via the Au−S bond. The photocurrent increased and an electrochemical oxidation peak current of MB was obtained because MB was close to the electrode surface. When the antibody-labeled ssDNA (Ab1-S1-Fc) was introduced onto the electrode surface, the hybridization between S0-MB and Ab1-S1-Fc occurred, making the MB probe move away from and the Fc probe come close to the electrode surface. This results in a decrease of the electrochemical oxidation peak current of MB and an increase of the electrochemical oxidation peak current of Fc. Meanwhile, the photocurrent of the electrode decreased obviously due to the enhancement effect of MB and inhibition effect of Fc toward the Au NPs/PTCDA@C_{60}/ITO photoelectrode. Afterward, the presence of CYFRA21-1 and antibody-labeled ssDNA (Ab2-S2) triggered a typical antigen−antibody sandwich immune reaction (Ab1, CYFRA21-1, and Ab2) and proximity hybridization between Ab1-S1-Fc and Ab2-S2, which not only caused the release of Ab1-S1-Fc from the electrode but also transformed S0-MB into a hairpin structure. These led to a decrease (an increase) of the oxidation peak current of Fc (MB) and an increase of the photocurrent of the electrode. Thus, CYFRA21-1 could be sensitively detected by the developed EC−PEC dual-mode sensing platform. By altering particular antibodies, the proposed dual-mode biosensor can be easily expanded to detect other biomarkers and may have potential applications in biological analysis and early disease diagnosis.

EXPERIMENTAL SECTION

Materials and Reagents. CYFRA21-1, two antibodies of CYFRA21-1 (Ab1 and Ab2), vascular endothelial growth factor (VEGF165), carcinoembryonic antigen (CEA), carbohydrate antigen 125 (CA125), and neuron-specific enolase (NSE) were acquired from Shanghai Linc-Bio Science Co. Ltd. (Shanghai, China). Perylene-3,4,9,10-tetracarboxylic dianhydride (PTCDA), fullerene (C_{60}) (99.5%), bovine serum albumin (BSA), 6-mercapto-1-hexanol (MCH), and gold chloride ($HAuCl_4{\cdot}4H_2O$) were bought from Sigma-Aldrich. Potassium ferrocyanide ($[K_4Fe(CN)_6]$), potassium ferricyanide ($[K_3Fe(CN)_6]$), glutaraldehyde (GA), and ascorbic acid (AA) were purchased from Sinopharm Chemical Reagent Co., Ltd. (China). Human serum was purchased from Anyan Inc. (China). The oligonucleotides (S0-MB: 5′-MB-CGC GTT AAC ATA CAA TAG ATC GCG-$(CH_2)_6$-SH; S1-Fc: 5′-Fc-GCG GAT CTA TTG TAT CAC ATA TTT TTT TTT TTT TTT TTT CAC CGT ATG CTA CTG TAG AT-NH_2; S2: NH_2-TAG GAA AAG GAG GAG GGT GGT TTT TTT TTT TTT TTT TTT TTA GAT ACA ATA GAT C) were obtained from Shanghai Sangon Biotech Co., Ltd. (Shanghai, China). The ITO slices (coating thickness, 180 ± 25 nm; sheet resistance, <10 Ω/sq) were supplied by Zhuhai Kaivo Electronic Components Co., Ltd (China). Ultrapure water (18.2 MΩ cm) provided by a Milli-Q filtration system (Millipore Corp., Bedford, MA) was used throughout this work.

Apparatus. The morphologies of the samples were characterized by scanning electron microscopy (SEM) (Hitachi S-4800, Japan). UV−visible (UV−vis) spectra were recorded on a UV-2100 spectrophotometer (Beijing Lab Tech, China). Photoelectrochemical (PEC) measurements, electrochemical impedance spectroscopy (EIS), and square wave voltammetry (SWV) experiments were performed on an electrochemical workstation (CHI 660D, China) with a three-electrode system including a modified ITO electrode (diameter, 5.6 mm) as the working electrode, a platinum wire as the auxiliary electrode, and a saturated calomel electrode (SCE) as the reference electrode. Photoelectrochemical investigation was conducted with a 300 W Xe lamp fitted with a 420 nm UV filter (Perfect Light, Beijing) as the irradiation source at a light intensity of 20 mW/cm^2. Here, the 420 nm UV filter was used to avoid the possible damage to biomolecules caused by UV rays.[36]

Preparation of Antibody-Labeled Single-Stranded DNA. The antibody-labeled ssDNA used in this work were prepared as follows: The antibodies of CYFRA21-1 (Ab1 or Ab2, 2 mg/mL) were reacted with GA in phosphate buffer (PBS, 100 mM, pH 7.4) at 4 °C for 15 min to obtain the GA-functionalized antibody. Then, the GA-functionalized Ab1 (5

https://doi.org/10.1021/acs.analchem.1c00746
Anal. Chem. 2021, 93, 6801−6807

μg/mL) was mixed with Fc-labeled (S1-Fc) (1 μM) under stirring for 30 min to get Ab1-S1-Fc through the chemical cross-linking reaction between GA and amino-modified DNA. The Ab2-labeled DNA (Ab2-S2) was also synthesized according to the above procedure. The resulting Ab1-S1-Fc and Ab2-S2 were stored at 4 °C for further use.

Preparation of C_{60}-Functionalized PTCDA (PTCDA@C_{60}). PTCDA was modified with C_{60} based on the π−π stacking interaction between PTCDA and C_{60}.[37,38] The preparation procedure is as follows: PTCDA (1 mg) was dispersed in ultrapure water (1.6 mL) and then the C_{60} solutions (0.4 mL) with different concentrations were added under stirring for 12 h. The prepared PTCDA@C_{60} solution (2.0 mL) with 0.5 mg/mL PTCDA and different concentrations of C_{60} were stored at 4 °C when not in use.

Preparation of the Dual-Mode Biosensor. Before modification, the ITO electrode was washed ultrasonically in acetone, ethanol/1 M NaOH (1:1, v/v), and ultrapure water in sequence, and then dried in air. After that, the ITO electrode was coated with PTCDA@C_{60} solution (25 μL) and then dried in air at room temperature. Next, in 1% $HAuCl_4$ solution, Au nanoparticles (Au NPs) were deposited on the PTCDA@C_{60} modified electrode at −0.2 V for 30 s. Subsequently, S0-MB (20 μL, 1 μM) was immobilized on the Au NPs/PTCDA@C_{60}/ITO electrode via the Au−S bond at 4 °C for 8 h. To block the nonspecific binding sites, the S0-MB/Au NPs/PTCDA@C_{60}/ITO electrode was incubated with MCH solution (20 μL, 1 mM) for 30 min at room temperature. The resulting electrode was further incubated with Ab1-S1-Fc solution (20 μL, 1 μM) including 0.5 wt % BSA for 2 h at room temperature. Finally, the obtained electrode (Ab1-S1-Fc/MCH/S0-MB/Au NPs/PTCDA@C_{60}/ITO) was stored in the dark at 4 °C for future use.

EC−PEC Dual-Mode Assay of CYFRA21-1. For CYFRA21-1 assay, the Ab1-S1-Fc/MCH/S0-MB/Au NPs/PTCDA@C_{60}/ITO electrode was incubated with the solution of Ab2-S2 (1 μM), CYFRA21-1 with different concentrations, and BSA (0.5 wt %) at 37 °C for 1 h. After that, the PEC assay was performed in PBS (100 mM, pH 7.4) containing 0.1 M ascorbic acid (AA) at an applied potential of 0 V. Furthermore, the SWV responses were recorded in PBS (100 mM, pH 7.4) from −0.45 to +0.6 V at a frequency of 15 Hz and an amplitude of 25 mV. On the other hand, the EIS experiments were carried out in 0.1 M KCl containing 5 mM $[Fe(CN)_6]^{3-/4-}$ with a frequency range from 10^5 to 0.1 Hz and an amplitude of 5 mV.

RESULTS AND DISCUSSION

Characterization of PTCDA@C_{60} and Au NPs/PTCDA@C_{60}/ITO Electrodes. Figure 1A shows the UV−vis absorption spectra of PTCDA and PTCDA@C_{60}. Obviously, the absorption intensity of PTCDA@C_{60} is stronger than that of pure PTCDA over the whole wavelength range, especially from 400 to 700 nm. This indicates that C_{60} has a sensitization effect on PTCDA and PTCDA@C_{60} may have good photoelectric behavior in the visible light range.

The morphologies of the ITO, PTCDA@C_{60}/ITO, and Au NPs/PTCDA@C_{60}/ITO electrodes have been characterized by scanning electron microscopy (SEM). A short rod-like morphology of PTCDA@C_{60} is observed and should originate from the PTCDA crystal (SI Figure S1B). On comparing Figure 1B with SI Figure S1, it is noted that Au NPs are

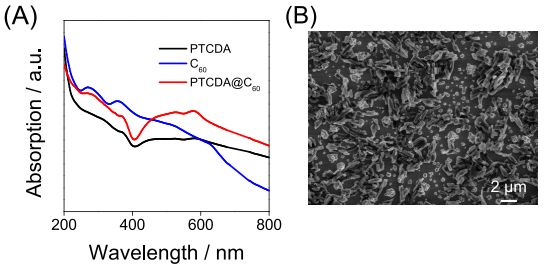

Figure 1. (A) UV−vis absorption spectra of PTCDA and PTCDA@C_{60}. (B) SEM image of Au NPs/PTCDA@C_{60}/ITO.

deposited on the surfaces of both ITO and PTCDA@C_{60}, and the average diameter of Au NPs is about 220 nm.

Electrochemical and Photoelectrochemical Investigations of the Developed Dual-Mode Biosensor. EIS is a powerful tool to monitor the stepwise preparation process of an electrode and the semicircle diameter of the Nyquist diagram of EIS is associated with the interfacial charge transfer resistance (R_{ct}). Here, the preparation procedure of the developed dual-mode biosensor is monitored by EIS, and the corresponding results are shown in Figure 2A. As shown in Figure 2A, the ITO electrode shows a small semicircle (curve a), indicating a rapid charge transfer process. When the ITO electrode is modified with PTCDA@C_{60}, the R_{ct} value of the electrode increases because of the low electrical conductivity of PTCDA@C_{60} (curve b). Further modification of Au NPs on the PTCDA@C_{60}/ITO electrode makes the R_{ct} value of the electrode decrease (curve c) because of the good electrical conductivity of Au NPs. The immobilization of S0-MB on the Au NPs/PTCDA@C_{60}/ITO electrode via the Au−S bond results in an increase of the R_{ct} value (curve d) owing to the electrostatic repulsion between the negatively charged DNA and the anionic redox probe ($[Fe(CN)_6]^{3-/4-}$). Due to the low conductivity of MCH and Ab1-S1-Fc, the R_{ct} values of the electrodes (curves e and f) increase further after the electrode is modified with MCH and Ab1-S1-Fc. However, when the electrode is incubated with CYFRA21-1 and Ab2-S2 solution, the R_{ct} value of the electrode decreases (curve g). This is because Ab1-S1-Fc is released from the electrode surface because of the formation of the Ab1-S1-Fc/CYFRA21-1/Ab2-S2 complex through the antigen−antibody sandwich immune reaction between CYFRA21-1 and its antibodies (Ab1 and Ab2) and proximity hybridization between S1 and S2. These results show that the proposed dual-mode biosensor is successfully prepared according to Scheme 1.

The electrochemical and photoelectrochemical performances of the various electrodes have also been investigated. As shown in Figure 2B, the bare ITO (curve a), PTCDA@C_{60}/ITO (curve b), and Au NPs/PTCDA@C_{60}/ITO (curve c) electrodes show no significant peak current signals. After the immobilization of S0-MB on the Au NPs/PTCDA@C_{60}/ITO electrode, an oxidation current peak is observed at −0.24 V (curve d) as the MB label approaches the Au NPs/PTCDA@C_{60}/ITO electrode. The introduction of the nonconductive MCH to the electrode slightly weakens the oxidation peak current of MB (curve e). When the electrode is further incubated with Ab1-S1-Fc, the hybridization between S0-MB and Ab1-S1-Fc occurs and makes the MB move away from and the Fc close to the electrode surface, resulting in that the MB oxidation peak current (at −0.24 V) decreases and a new oxidation peak (known as the oxidation peak of Fc) appears at

https://doi.org/10.1021/acs.analchem.1c00746
Anal. Chem. 2021, 93, 6801−6807

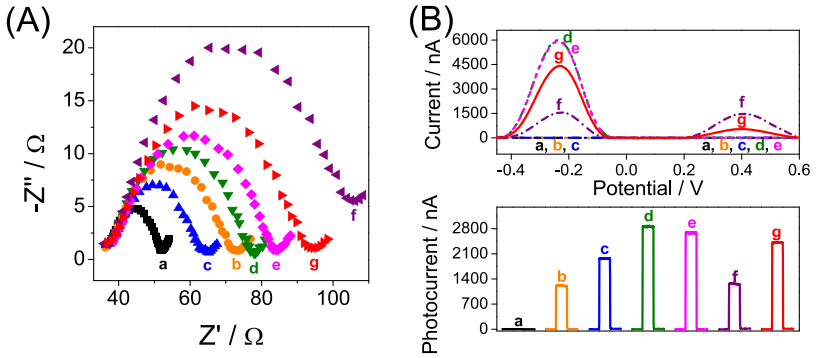

Figure 2. (A) EIS results of different electrodes in 0.1 M KCl aqueous solution containing 5 mM $[Fe(CN)_6]^{3-/4-}$ (1:1) in the frequency range from 10^5 to 0.1 Hz. (B) SWV responses of different electrodes in PBS (100 mM, pH 7.4) and PEC responses of different electrodes in PBS (100 mM, pH 7.4) containing 0.1 M AA at 0 V. (a) ITO, (b) PTCDA@C_{60}/ITO, (c) Au NPs/PTCDA@C_{60}/ITO, (d) S0-MB/Au NPs/PTCDA@C_{60}/ITO, (e) MCH/S0-MB/Au NPs/PTCDA@C_{60}/ITO, (f) Ab1-S1-Fc/MCH/S0-MB/Au NPs/PTCDA@C_{60}/ITO, and (g) Ab1-S1-Fc/MCH/S0-MB/Au NPs/PTCDA@C_{60}/ITO electrodes incubated with 1 ng/mL CYFRA21-1 and Ab2-S2.

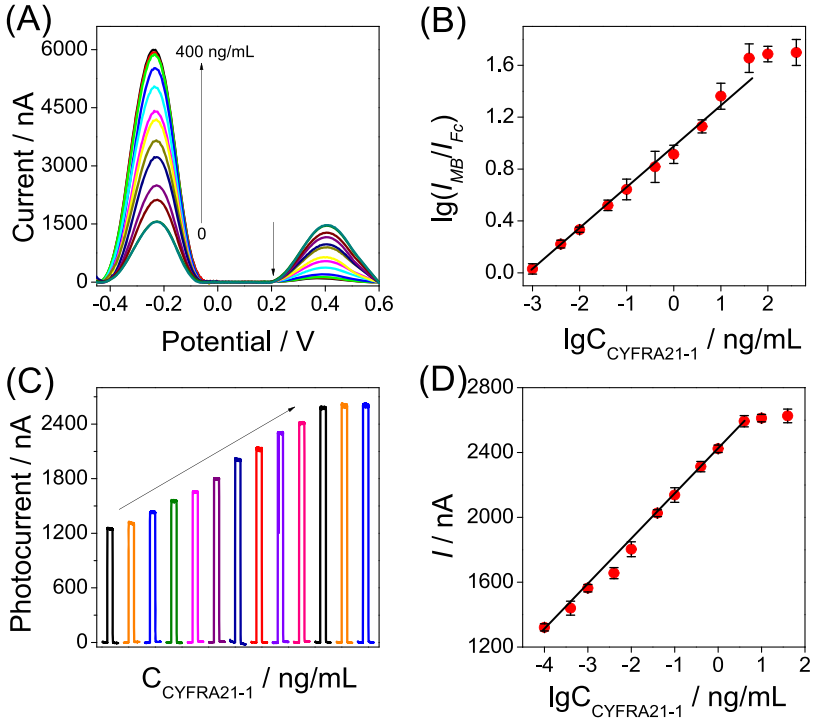

Figure 3. (A) SWV responses of the developed dual-mode biosensor toward various concentrations of CYFRA21-1: 0, 0.001, 0.004, 0.01, 0.04, 0.1, 0.4, 1, 4, 10, 40, 100, and 400 ng/mL. (B) Linear relationship between logarithm of I_{MB}/I_{Fc} and logarithm of CYFRA21-1 concentration. (C) PEC responses of the developed dual-mode biosensor toward various concentrations of CYFRA21-1: 0, 0.0001, 0.0004, 0.001, 0.004, 0.01, 0.04, 0.1, 0.4, 1, 4, 10, and 40 ng/mL. (D) Linear relationship between photocurrent and logarithm of CYFRA21-1 concentration.

0.4 V (curve f). In the presence of CYFRA21-1 and Ab2-S2, the immune reaction of the Ab1-target-Ab2 triggers the proximity hybridization between S1 and S2, resulting in the release of Ab1-S1-Fc from the electrode surface and the regeneration of the hairpin structure of S0-MB. As a result, the oxidation peak current of MB (at −0.24 V) increases, and the oxidation peak current of Fc (at 0.4 V) decreases (curve g). On the other hand, the PEC responses of different electrodes are shown in Figure 2B. Note that the bare ITO electrode (curve a) has no obvious photocurrent signal. However, a photocurrent response can be observed on the PTCDA@C_{60}/ITO electrode (curve b) due to the good photoelectric properties of the PTCDA@C_{60} composite. The Au NPs deposited electrochemically on the PTCDA@C_{60}/ITO electrode further increases the photocurrent of the electrode due to the good electron transfer capability of Au NPs (curve c). When S0-MB is immobilized on the Au NPs/PTCDA@C_{60}/ITO electrode via the Au−S bond, the photocurrent increases obviously due to the approaching of the sensitizer (MB) to the PTCDA@C_{60} composite.[39,40] Further modification of MCH weakens the photocurrent signal slightly due to the blocking effect of MCH (curve e). After this, the hybridization between S0-MB and Ab1-S1-Fc makes the photocurrent decrease sharply due to the weakening of the enhancing effect of MB and the strengthening of the inhibiting effect of Fc on the Au NPs/PTCDA@C_{60}/ITO electrode (curve f). The possible charge transfer routes are shown in SI Scheme S1. After the addition of CYFRA21-1 and Ab2-S2, the photocurrent of the electrode increases obviously (curve g) because the hairpin structure of S0-MB is formed again and Ab1-S1-Fc is released from the

https://doi.org/10.1021/acs.analchem.1c00746
Anal. Chem. 2021, 93, 6801−6807

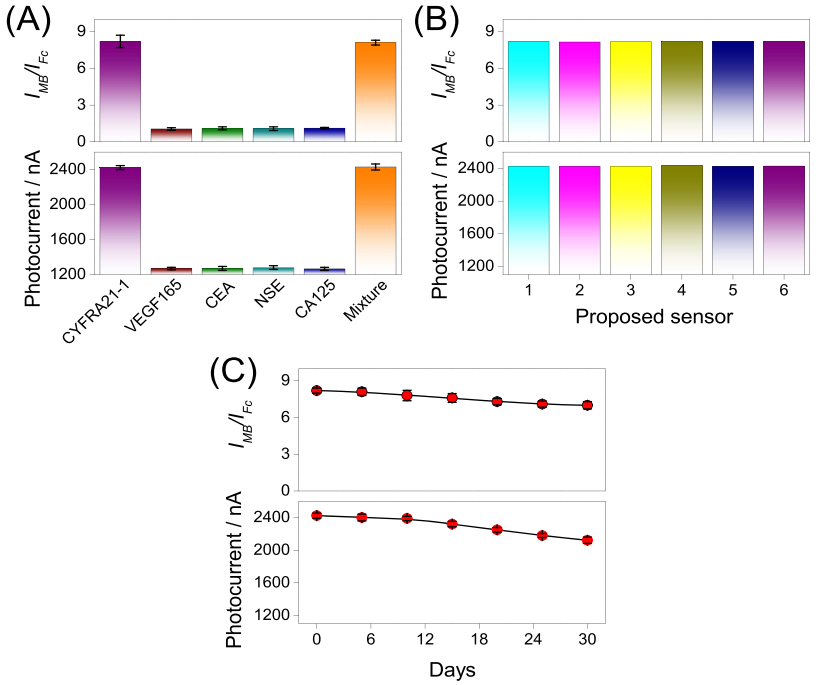

Figure 4. (A) Specificity of the developed EC−PEC dual-mode biosensor for CYFRA21-1 (1 ng/mL) detection over other interfering antigens, including VEGF165 (1 ng/mL), CEA (1 ng/mL), NSE (1 ng/mL), and CA125 (1 U/mL). (B) Reproducibility of the dual-mode biosensor in the same batch. (C) The storage stability of the dual-mode biosensor examined every 5 days for 30 days.

electrode surface via the immune reaction of the Ab1-target-Ab2 and proximity hybridization between S1 and S2. Based on the above results, the developed sensing platform has been established successfully according to Scheme 1 and CYFRA21-1 can be detected sensitively by this dual-signaling electrochemical ratiometric strategy and on−off−on PEC method.

Electrochemical and Photoelectrochemical Assay of CYFRA21-1. Under the optimal conditions (SI Figures S2 and S3), the developed EC and PEC biosensing platform was used for CYFRA21-1 assay. As the concentration of CYFRA21-1 increases, the oxidation peak current of MB (Fc) increases (decreases) and the photocurrent increases (Figure 3A,C). The results show that the logarithm of the ratio of the oxidation peak currents of MB to Fc has a good linear relationship with the logarithm of the CYFRA21-1 concentration in the concentration range of 0.001−40 ng/mL ($\lg(I_{MB}/I_{Fc}) = 0.317\lg[\text{CYFRA21-1}] + 0.970$, $R^2 = 0.9921$) (Figure 3B). In the range of 0.0001−4 ng/mL, the photocurrent also has a good linear relationship with the logarithm of the CYFRA21-1 concentration ($I = 218.5\lg[\text{CYFRA21-1}] + 2414.2$, $R^2 = 0.9949$) (Figure 3D). Furthermore, the limits of detection (LOD, S/N = 3) of EC and PEC are calculated to be 0.3 and 0.03 pg/mL, respectively. It is noted that the developed dual-mode method can be used to identify the cut-off value of CYFRA21-1 in 3.3 ng/mL serum in NSCLC.[41] On the other hand, the developed dual-mode biosensor shows a lower detection limit than most other reported methods (SI Table S1).

Selectivity, Reproducibility, and Stability. Selectivity is a key factor for assessing the practicality of the developed biosensing platform. Several possible interferents, VEGF165, CEA, NSE, and CA125 were utilized to evaluate the selectivity of the dual-mode biosensing platform (Figure 4A). In the presence of CYFRA21-1, the obvious EC and PEC responses are obtained, but no significant changes are observed in the presence of other antigens. Also, the EC and PEC signals are not affected obviously when CYFRA21-1 is mixed with other antigens. These indicate that the dual-mode biosensor has good selectivity and can resist the interference of other antigens. On the other hand, the PEC responses of the biosensing platform under 10 "on" and "off" irradiation cycles (SI Figure S4) are studied and show good PEC stability. Furthermore, the reproducibility and stability of the dual-mode biosensor were also evaluated. For 1 ng/mL CYFRA21-1, the relative standard deviation (RSD) value of EC responses on six independent electrodes is 2.4%, and the RSD value of PEC responses is 2.2% (Figure 4B). Moreover, the developed dual-mode biosensing platform was stored at 4 °C for 30 days to investigate its stability. The EC response is still 85.4% and the PEC response is still 87.6% of the initial values (CYFRA21-1, 1 ng/mL) (Figure 4C). These results show that the dual-mode biosensor has acceptable reproducibility and stability.

Recovery Test of CYFRA21-1 in Serum. To investigate the analytical feasibility of the dual-mode biosensor in complex samples, the developed dual-mode sensor was used to analyze CYFRA21-1 in serum. Different concentrations of CYFRA21-1 were spiked in 10-fold diluted blank human serum samples, which were diluted with PBS (100 mM, pH 7.4). CYFRA21-1 in the serum was detected by EC and PEC methods of the proposed dual-mode biosensor, and the results are compared with those obtained from enzyme-linked immunosorbent assay (ELISA). As described in SI Table S2, the recoveries obtained from our developed EC−PC dual-mode sensing platform are acceptable and have good consistency with those from ELISA. These indicate that the developed dual-mode biosensor can mutually verify the measurement results obtained by the two methods, which further proves to effectively improve the accuracy and reliability of detection and has an excellent potentiality for CYFRA21-1 assay in complex samples.

https://doi.org/10.1021/acs.analchem.1c00746
Anal. Chem. 2021, 93, 6801−6807

CONCLUSIONS

In summary, a sensitive EC−PEC dual-mode biosensing platform has been developed based on the enhancing effect of MB and inhibiting effect of Fc on the photoelectric performance of the Au NPs/PTCDA@C_{60}/ITO electrode and electrochemical activities of MB and Fc at different potentials. The NSCLC marker CYFRA21-1 can be detected by either the dual-signaling electrochemical ratiometric strategy with a linear range of 0.001−40 ng/mL and the limit of detection of 0.3 pg/mL or the on−off−on PEC method with a linear range of 0.0001−4 ng/mL and the limit of detection of 0.03 pg/mL. In addition, the dual-mode biosensor has acceptable selectivity, stability, and reproducibility, as well as good applicability in human serum samples. Furthermore, by altering the particular antibody of disease-related biomarkers, the developed dual-mode biosensing platform can be readily extended to the assay of other tumor marker antigens, implying its great potential applications in biological analysis and early disease diagnosis.

ASSOCIATED CONTENT

Supporting Information

The Supporting Information is available free of charge at https://pubs.acs.org/doi/10.1021/acs.analchem.1c00746.

PEC mechanisms for the enhancing effect of MB and the inhibiting effect of Fc to the photocurrent of the Au NPs/PTCDA@C_{60}/ITO photoelectrode; SEM images of the ITO and PTCDA@C_{60}/ITO electrodes; optimization of experimental conditions; photocurrent stability of the biosensor; comparison of different methods for CYFRA21-1 assay; recovery assay of CYFRA21-1 in the human serum samples (PDF)

AUTHOR INFORMATION

Corresponding Author

Jinhua Chen − *State Key Laboratory of Chemo/Biosensing and Chemometrics, College of Chemistry and Chemical Engineering, Hunan University, Changsha 410082, P. R. China;* orcid.org/0000-0001-5089-0927; Phone: +86-731-88821848; Email: chenjinhua@hnu.edu.cn

Authors

Qingqing Zhang − *State Key Laboratory of Chemo/Biosensing and Chemometrics, College of Chemistry and Chemical Engineering, Hunan University, Changsha 410082, P. R. China*

Yamin Fu − *State Key Laboratory of Chemo/Biosensing and Chemometrics, College of Chemistry and Chemical Engineering, Hunan University, Changsha 410082, P. R. China*

Ke Xiao − *State Key Laboratory of Chemo/Biosensing and Chemometrics, College of Chemistry and Chemical Engineering, Hunan University, Changsha 410082, P. R. China*

Cuicui Du − *State Key Laboratory of Chemo/Biosensing and Chemometrics, College of Chemistry and Chemical Engineering, Hunan University, Changsha 410082, P. R. China*

Xiaohua Zhang − *State Key Laboratory of Chemo/Biosensing and Chemometrics, College of Chemistry and Chemical Engineering, Hunan University, Changsha 410082, P. R. China*

Complete contact information is available at: https://pubs.acs.org/10.1021/acs.analchem.1c00746

Notes

The authors declare no competing financial interest.

ACKNOWLEDGMENTS

This work was financially supported by NSFC (22074033 and 21727810).

REFERENCES

(1) Kitano, H. *Science* **2002**, *295*, 1662−1664.
(2) Senel, M.; Dervisevic, E.; Alhassen, S.; Dervisevic, M.; Alachkar, A.; Cadarso, V. J.; Voelcker, N. H. *Anal. Chem.* **2020**, *92*, 12347−12355.
(3) Fu, Y. M.; Xiao, K.; Zhang, X. H.; Du, C. C.; Chen, J. H. *Anal. Chem.* **2021**, *93*, 1076−1083.
(4) Xiao, L. P.; Zhu, A. M.; Xu, Q. C.; Chen, Y.; Xu, J.; Weng, J. *ACS Appl. Mater. Interfaces* **2017**, *9*, 6931−6940.
(5) Yang, H. T.; Li, P.; Wang, D. Z.; Liu, Y.; Wei, W.; Zhang, Y. J.; Liu, S. Q. *Anal. Chem.* **2019**, *91*, 11038−11044.
(6) Nie, Y. M.; Yuan, X. D.; Zhang, P.; Chai, Y. Q.; Yuan, R. *Anal. Chem.* **2019**, *91*, 3452−3458.
(7) Kenry; Geldert, A.; Zhang, X.; Zhang, H.; Lim, C. T. *ACS Sens.* **2016**, *1*, 1315−1321.
(8) Lu, Y. W.; Zhao, H.; Fan, G. C.; Luo, X. L. *Biosens. Bioelectron.* **2019**, *142*, No. 111569.
(9) Gao, X. H.; Li, H. K.; Zhao, Y.; Jie, G. F. *Biosens. Bioelectron.* **2019**, *143*, No. 111602.
(10) Wei, J.; Chang, W. D.; Qileng, A.; Liu, W. P.; Zhang, Y.; Rong, S. Y.; Lei, H. T.; Liu, Y. J. *Anal. Chem.* **2018**, *90*, 9606−9613.
(11) Mei, L.-P.; Jiang, X.-Y.; Yu, X.-D.; Zhao, W.-W.; Xu, J. J.; Chen, H.-Y. *Anal. Chem.* **2018**, *90*, 2749−2755.
(12) Mars, A.; Hamami, M.; Bechnak, L.; Patra, D.; Raouafi, N. *Anal. Chim. Acta* **2018**, *1036*, 141−146.
(13) Xu, X. M.; Hou, R. Z.; Gao, P. C.; Miao, M.; Lou, X. D.; Liu, B. F.; Xia, F. *Anal. Chem.* **2016**, *88*, 2386−2391.
(14) Deng, H. M.; Chai, Y. Q.; Yuan, R.; Yuan, Y. L. *Anal. Chem.* **2020**, *92*, 8364−8370.
(15) Shang, H. Y.; Xu, H.; Jin, L. J.; Wang, C.; Chen, C. Y.; Song, T. X.; Du, Y. K. *Biosens. Bioelectron.* **2020**, *159*, No. 112202.
(16) Zhu, C. X.; Liu, M. Y.; Li, X. Y.; Zhang, X. H.; Chen, J. H. *Chem. Commun.* **2018**, *54*, 10359−10362.
(17) Xiong, E. H.; Zhang, X. H.; Liu, Y. Q.; Zhou, J. W.; Yu, P.; Li, X. Y.; Chen, J. H. *Anal. Chem.* **2015**, *87*, 7291−7296.
(18) Xiong, E. H.; Li, Z. Z.; Zhang, X. H.; Zhou, J. W.; Yan, X. X.; Liu, Y. Q.; Chen, J. H. *Anal. Chem.* **2017**, *89*, 8830−8835.
(19) Du, Y.; Lim, B. J.; Li, B.; Jiang, Y. S.; Sessler, J. L.; Ellington, A. D. *Anal. Chem.* **2014**, *86*, 8010−8016.
(20) Chai, X.; Zhou, X.; Zhu, A.; Zhang, L.; Qin, Y.; Shi, G.; Tian, Y. *Angew. Chem., Int. Ed.* **2013**, *52*, 8129−8133.
(21) Zhao, L.; Sun, R.; He, P.; Zhang, X. *Anal. Chem.* **2019**, *91*, 14773−14779.
(22) Ding, C.; Wang, X.; Luo, X. *Anal. Chem.* **2019**, *91*, 15846−15852.
(23) Liu, Q.; Huan, J.; Hao, N.; Qian, J.; Mao, H.; Wang, K. *ACS Appl. Mater. Interfaces* **2017**, *9*, 18369−18376.
(24) Li, C.; Wang, H.; Shen, J.; Tang, B. *Anal. Chem.* **2015**, *87*, 4283−4291.
(25) Zhao, W.-W.; Wang, J.; Zhu, Y.-C.; Xu, J.-J.; Chen, H.-Y. *Anal. Chem.* **2015**, *87*, 9520−9531.
(26) Zhao, W.-W.; Xu, J.-J.; Chen, H.-Y. *Chem. Rev.* **2014**, *114*, 7421−7441.
(27) Wen, G. M.; Yang, X. J.; Wang, Y. Z. *J. Mater. Chem. B* **2017**, *5*, 7775−7780.
(28) Wang, F. X.; Ye, C.; Mo, S.; Liao, L. L.; Luo, H. Q.; Li, N. B. *Sens. Actuators, B* **2019**, *288*, 202−209.
(29) Fu, Y. M.; Ding, F.; Chen, J. H.; Liu, M. Y.; Zhang, X. H.; Du, C. C.; Si, S. H. *Chem. Commun.* **2020**, *56*, 5799−5802.

(30) Meng, L. X.; Liu, M. Y.; Xiao, K.; Zhang, X. H.; Du, C. C.; Chen, J. H. *Chem. Commun.* **2020**, *56*, 8261−8264.
(31) Qian, Y. R.; Feng, J. H.; Xu, R.; Fan, D. W.; Du, Y.; Ren, X.; Wei, Q.; Ju, H. X. *ACS Appl. Mater. Interfaces* **2020**, *12*, 16662−16669.
(32) Zhu, M. H.; Zhong, X.; Deng, H. M.; Huang, L. J.; Yuan, R.; Yuan, Y. L. *Biosens. Bioelectron.* **2019**, *143*, No. 111618.
(33) Li, M. J.; Zheng, Y. N.; Liang, W. B.; Yuan, Y. L.; Chai, Y. Q.; Yuan, R. *Chem. Commun.* **2016**, *52*, 8138−8141.
(34) Holdenrieder, S.; von Pawel, J.; Dankelmann, E.; Duell, T.; Faderl, B.; Markus, A.; Siakavara, M.; Wagner, H.; Feldmann, K.; Hoffmann, H.; Raith, H.; Nagel, D.; Stieber, P. *Lung Cancer* **2009**, *63*, 128−135.
(35) McKeegan, E. M.; Ansell, P. J.; Davis, G.; Chan, S.; Chandran, R. K.; Gawel, S. H.; Dowell, B. L.; Bhathena, A.; Chakravartty, A.; McKee, M. D.; Ricker, J. L.; Carlson, D. M.; Ramalingam, S. S.; Devanarayan, V. *Lung Cancer* **2015**, *90*, 296−301.
(36) Zhu, A. W.; Luo, Y. P.; Tian, Y. *Anal. Chem.* **2009**, *81*, 7243−7247.
(37) Zhang, Z. X.; Huang, H. L.; Yang, X. M.; Zang, L. *J. Phys. Chem. Lett.* **2011**, *2*, 2897−2905.
(38) Miao, Y. Y.; Xu, J.; Shen, Y.; Chen, L.; Bian, Y. P.; Hu, Y.; Zhou, W.; Zheng, F.; Man, N.; Shen, Y. Y.; Zhang, Y. J.; Wang, M.; Wen, L. P. *ACS Nano* **2014**, *8*, 6131−6144.
(39) Long, D.; Li, M. J.; Wang, H. H.; Wang, H. J.; Chai, Y. Q.; Yuan, R. *Biosens. Bioelectron.* **2019**, *142*, No. 111579.
(40) Huang, L. J.; Deng, H. M.; Zhong, X.; Zhu, M. H.; Chai, Y. Q.; Yuan, R.; Yuan, Y. L. *Biosens. Bioelectron.* **2019**, *145*, No. 111702.
(41) Hur, J.; Lee, H. J.; Nam, J. E.; Kim, Y. J.; Hong, Y. J.; Kim, H. Y.; Kim, S. K.; Chang, J.; Kim, J. H.; Chung, K. Y.; Lee, H. S.; Choi, B. W. *BMC Cancer* **2012**, *12*, No. 392.

https://doi.org/10.1021/acs.analchem.1c00746
Anal. Chem. 2021, 93, 6801−6807